An Evaluation of Simultaneous Dual-Tracer Technique for PET Static Studies

Francisca P. Figueiras, Xavier Jimenez, Deborah Pareto, Vanessa Gómez, Jordi Llop, Juan D. Gispert

Abstract– **Simultaneous dual-tracer technique (SDTT) was proposed 30 years ago to discriminate between two PET radiotracer concentrations based on their different radioactive decay rates. This study evaluates the performance of SDTT in static studies using 2-deoxy-2-^{18}F-fluoro-D-glucose (^{18}F-FDG) and ^{13}N-Amonium (^{13}N-NH$_4^+$) as radiotracers. SDTT was applied to a phantom. The influence of applying SDTT on either the reconstructed image or directly on the sinogram, different rebinning algorithms, total time acquisition and frame duration were investigated. Best results were obtained using the image method with a single-slice rebinning (SSRB) and total time acquisition of at least 20 min. Using the reasonable experimental settings better per-voxel statistics are achieved and subsequently SDTT has a better performance. Frame duration did not influence SDTT. The results encourage the use of SDTT as it has very good potential for simultaneously examining two different biological processes at the same time utilizing rodent PET scanners.**

I. INTRODUCTION

POSITRON Emission Tomography (PET) and Single Photon Emission Computed Tomography (SPECT) are nuclear medicine imaging techniques, which produce a three dimensional image of functional processes in the body. They measure *in vivo* the biodistribution of imaging agents labelled with radionuclides, which are called radiotracers. SPECT allows for dual-tracer acquisitions, to simultaneously image the distribution of two radiotracers in the body. In this technique, two tracers labelled with nuclides with different photon energies are introduced into the patient, and the separation of these two tracers is achieved by energy discrimination [1-3]. Because the two tracers are in the body at the same time and are measured simultaneously, the dual tracer technique can reduce problems of patient movement, image alignment and physiologic changes.

In PET, however, the technique of energy discrimination is not applicable, since photons emitted from the annihilation of positrons have the same energy (511 KeV). To overcome this limitation, tracer discrimination using radioactive decay rates of different positron emitters was originally proposed in [4]. Nevertheless, this procedure is not routinely applied since it enhances the noise in the images, as a function of the relative half-lives of the isotopes and the time duration of the scans as studied in [5].

Dual-tracer PET studies are of clinical interest but they require two separate scans. E.g. a myocardial viability examination requires the assessment of glucose consumption (2-deoxy-2-^{18}F-fluoro-D-glucose scan) and perfusion (^{13}N-Amonium scan). Simultaneous imaging techniques reduce the problems related to image alignment and physiologic changes inherent in successive imaging. Other sequential and simultaneous dual-tracer PET scans have been also investigated [4-9]. E.g. PET kinetic analysis with dual-tracer injection, where the aim of the work was to investigate the optimal injection intervals and administration dose ratios of the two tracers [6-8].

The basis of the simultaneous dual-tracer technique (SDTT) is to discriminate each radiotracer using their different radioactive decay rates. This technique can be performed at the dynamic sinogram or image levels. This study describes and compares these two different methods of simultaneous dual-tracer technique: the Sinogram Method (SM) and the Image Method (IM). SDTT was performed on both phantom and *in vivo* data, using 2-deoxy-2-^{18}F-fluoro-D-glucose (^{18}F-FDG) and ^{13}N-Amonium (^{13}N-NH$_4^+$) radiotracers with half-life times of 9.97 and 109.77 minutes for ^{13}N and ^{18}F respectively. The aim of this study was to assess to what extent the experimental settings could influence the SDTT results. The impact on the SDTT of some frequent experimental settings, such as rebinning algorithms, the total acquisition time and the frame duration were also investigated individually for both methods.

II. MATERIALS AND METHODS

A. Theory

Dynamic PET imaging of two radionuclides with decay constants λ_A and λ_B with initial (t=0) activity concentrations m_A and m_B, will yield an observed activity m along n time frames:

$$m(x,y,z,t_i) = m_A(x,y,z,0)\cdot e^{-\lambda A \cdot tA} + m_B(x,y,z,0)\cdot e^{-\lambda B \cdot tB} \quad (i=1,\ldots,n) \quad (1)$$

where m_A and m_B can be estimated using the non-linear least-squares fitting method [10]. In this study the unknown parameters were estimated using the non-linear least-squares

data fitting by the Gauss-Newton method, using MATLAB software (The MathWorks Inc., Natick, MA, USA).

The above described method can be applied to dynamic sinograms or directly to the reconstructed dynamic images. This study analysed and compared these two different methods of SDTT. The first method is the Sinogram Method (SM) that consists of using the dynamic sinogram of the dual-tracer acquisition as initial source. Because of the different radioactive decay rates of ^{18}F and ^{13}N, from the dynamic sinogram and using a non-linear least squares fitting method, it is possible to determine the two static sinograms that correspond to the ^{18}F-FDG and ^{13}N-NH$_4^+$ radiotracers. Subsequently, both images were reconstructed and analysed. The second method, the Image Method (IM), differs from the previous one in that it uses the resulting dynamic image of the dual-tracer PET acquisition as source, providing as result two static images that correspond to ^{18}F-FDG and ^{13}N-NH$_4^+$ radiotracers (Fig. 1).
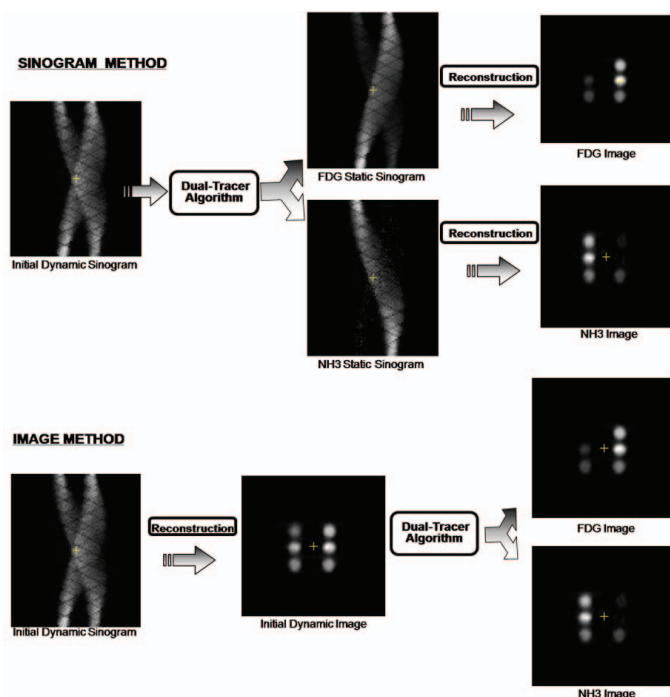

Fig 1. Scheme of both simultaneous dual-tracer technique methods: the Sinogram Method and the Image Method.

B. Phantom Experiments

In order to investigate the impact of the usual post-processing parameters in PET imaging, the standard filtered-backprojection (FBP) reconstruction algorithm was used and two different rebinning algorithms were applied: the single-slice rebinning (SSRB) and the Fourier rebinning (FORE). The single-slice rebinning (SSRB) was applied using different values for span and ring difference to evaluate their impact on the SDTT. This technique was also applied using different total time acquisition (5, 10, 20 and 30 min), different frame duration (10, 30, 60, 120, 300 seconds) and in consequence a different number of frames, in order to evaluate how these factors influence the results. Each parameter was studied

individually; each different rebinning algorithm was applied using different total time acquisition and frame duration.

SDTT was applied to a phantom of six eppendorf tubes that were filled with different relative concentrations of ^{18}F-FDG and ^{13}N-NH$_4^+$ and imaged for 33 min in a SIEMENS micro-PET R4. Because SDTT consists of the different radioactive decay rates of each radiotracer, no decay correction or attenuation were applied. The initial activity concentration of ^{18}F-FDG and ^{13}N-NH$_4^+$ was 12,58 MBq/ml (340 μCi/cc) and 6,475 MBq/ml (175 μCi/cc), respectively. The ratios of ^{18}F-FDG to ^{13}N-NH$_4^+$ volume that was introduced into each of the eppendorf tubes is shown in Fig 2.

Sinograms were histogrammed using both SSRB and 3D rebinning using the tomograph software. The dimensions were 84 x 96 and 63 planes. The 3D sinograms present 11 segments and the default span and ring difference settings for micro-PET R4 are 3 and 31, respectively. To the SSRB rebinning, the settings on the micro-PET protocol setup page give a ring difference of 15 and span of 31. In this study SSRB was applied using two different span and ring difference values: one, using the default values of the micro-PET protocol; and another one, using a span of 3 and a ring difference of 31.

Scans were reconstructed using the standard filtered-backprojection (FBP) with a ramp filter (cutoff frequency = 0.5 mm^{-1}), using an image matrix size of 128 x 128, resulting in images consisting of 63 planes with voxel size of 0.845247 x 0.845247 x 1.2115 mm^3. Reconstruction was implemented using both SSRB (also using two different span and ring difference values) and FORE. All data was corrected for random coincidences, dead time and normalization.
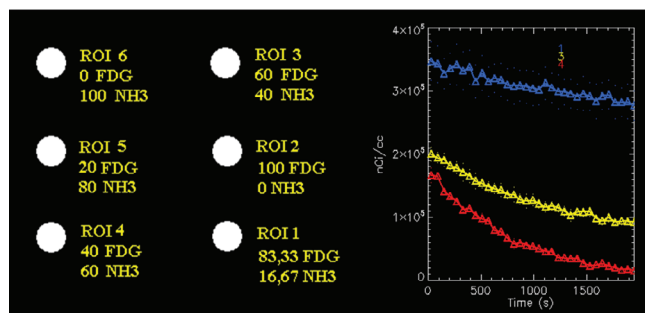

Fig 2. Relative volumes of ^{18}F-FDG and ^{13}N-NH$_4^+$ introduced on each eppendorf tube (left). Time-Activity Curves (TACs) of ^{18}F-FDG (blue), of ^{13}N-NH$_4^+$ (red) and of dual-isotope (yellow) (right).

C. Evaluation of SDTT

To evaluate quantitatively the results of both methods, the accuracy and the Signal to Noise Ratio (SNR) of their resulted images were measured and compared. Seven regions of interest (ROI) were drawn, one for each eppendorf tube and one for the background. The ROI of the background corresponds to the entire image except the six eppendorf ROIs (ROI$_{background}$ = Image − ROI$_{1:6}$).

From the number of counts of the dynamic image at t=0 (first frame) and the sum of the counts of the two static resulted images of ^{18}F-FDG and ^{13}N-NH$_4^+$ radiotracers, the accuracy of both methods was determined by the following expression:

$$A = \frac{N_{13N-NH3} + N_{18F-FDG}}{N_0} \times 100 \qquad (2)$$

where N_0 is the number of counts at t=0. From the number of counts of each ROI on both radiotracer images, it was possible to determine their concentration and to compare them with the initial concentrations present in the phantom.

The behaviour of the image noise in this process was also analysed. From the mean and standard deviation of each ROI, including the ROI of the background, the SNR was calculated using the hottest regions as reference:

$$SNR = \frac{\left(X_{Hot\,Region} - X_{Background}\right)}{\sigma_{Background}} \qquad (3)$$

where X is the mean of the ROI and σ its standard deviation [9]. The hottest regions correspond to the ROI containing only ^{18}F-FDG or ^{13}N-NH$_4^+$ (100% ^{18}F-FDG or 100% ^{13}N-NH$_4^+$).

III. RESULTS

A. Rebinning Algorithms

From Fig. 3, it can be observed that different rebinning algorithms applied to the SDTT lead to different results. E.g. using a SSRB sinogram with a span of 3 and ring difference of 31, an image with higher SNR is obtained (i.e., with less noise) than using a 3D sinogram and a Fourier rebinning reconstruction.
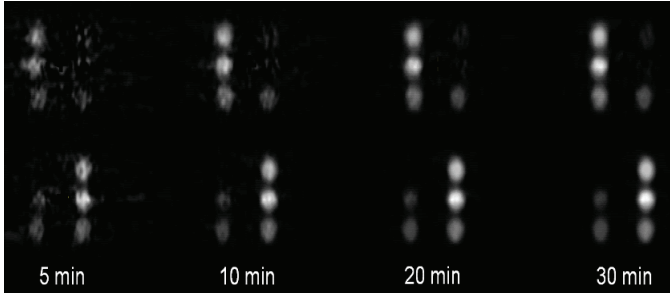
Fig 3. ^{13}N-NH$_4^+$ (upper row) and ^{18}F-FDG images for different rebinning algorithms: (left to right) SSRB with a span of 31 and a ring difference of 15; SSRB with a span of 3 and ring difference of 31; 3D Sinogram and FORE on the reconstruction. Experimental settings: total time acquisition of 30 min and frame duration of 60 sec.

This result can be explained by the fact that when using a 3D sinogram and a Fourier rebinning reconstruction, each voxel presents a lower number of counts, and therefore worse SNR, given the Poisson nature of noise in PET imaging. In contrast, if a SSRB sinogram is used, higher SNR values are achieved because of the better per-voxel counting statistics [10].

B. Total Time Acquisition and frame duration

Regarding to time acquisition, when the total time acquisition is above 20 min the resulting images are of a similar quality as the 30 min static image. For lower total time

acquisition, this procedure enhances noise in the images. The SNR values increase with longer total time acquisition (Fig. 4).
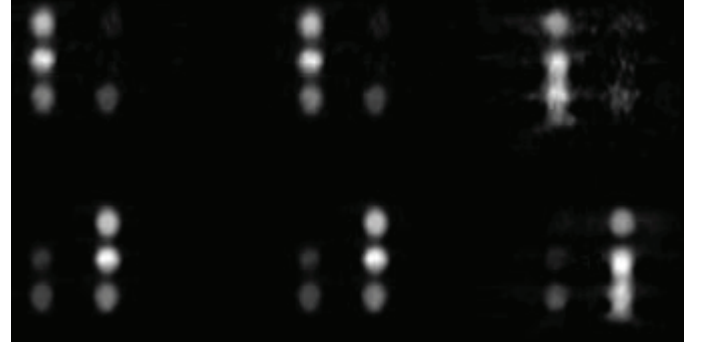
Fig 4. ^{13}N-NH$_4^+$ (upper row) and ^{18}F-FDG images for different total acquisition time: 5, 10, 20 and 30 min. Experimental settings: SSRB sinogram with a span of 3 and ring difference of 31 and frame duration of 60 sec.

The SNR of the initial image (^{18}F-FDG and ^{13}N-NH$_4^+$ combined; SSRB sinogram with a span of: 3; ring difference: 31; total time acquisition: 30 min.; frame duration: 60 sec.) was of 43.65 and, after applying the SDTT with the image method the resultant ^{18}F-FDG and ^{13}N-NH$_4^+$ images presented SNR values of 50.32 and 39.00, respectively, and when using the sinogram method 50.21 and 38.97, respectively. When time acquisition is 30 min, both methods discriminate ^{18}F-FDG and ^{13}N-NH$_4^+$ images with similar SNR values compared to the initial dynamic image. ^{18}F-FDG images present less noise than the initial dynamic image. In contrast the ^{13}N-NH$_4^+$ images are slightly noisier. E.g. applying SDTT using SSRB with a span of 3 and ring difference of 31, when the total time acquisition is between 20 and 30 min, the ^{18}F-FDG images SNR is approximately 50. In contrast, when the total time acquisition is 10 min the ^{18}F-FDG images present a SNR of 12.

In relation to frame duration, Figure 3 clearly shows that different frame duration does not influence the precision of SDTT. Independently of frame duration, the SNR values do not vary.

Both IM and SM methods discriminate ^{18}F-FDG and ^{13}N-NH$_4^+$ images with similar quality comparing to the initial dynamic image (Table 1). ^{18}F-FDG images present less noise than the initial dynamic image since ^{18}F-FDG signal hardly varies over total acquisition time, and therefore the noise is cancelled out when fitting the data. In contrast, ^{13}N-NH$_4^+$ images are slightly noisier due to two different facts: (i) ^{18}F-FDG signal hardly over time, therefore the noise is cancelled out when fitting the data. In contrast, ^{13}N-NH$_4^+$ varies to a higher extent and thus, together with the true ^{13}N-NH$_4^+$ signal, a slightly amount of noise is also captured. (ii) Nevertheless, the main factor to explain this difference between ^{18}F-FDG and ^{13}N-NH$_4^+$ images are their different initial activity concentration, ^{18}F-FDG activity concentration was approximately the double of ^{13}N-NH$_4^+$. Subsequently, there are fewer counts on the ^{13}N-NH$_4^+$ images, which also imply lower SNR. In addition, the images obtained with ^{18}F-FDG are usually better than with ^{13}N-NH$_4^+$. The accuracy in the measurement of the ^{13}N-NH$_4^+$ to ^{18}F-FDG ratios in the

resultant images after applying SDTT were over 99,98% for the Image Method and over 97.50% for the Sinogram Method. As it can be observed, both images were correctly separated and as expected ^{13}N-NH$_4^+$ image is slightly noisier than ^{18}F-FDG image.

C. Image Method vs Sinogram Method

The accuracy of the IM using a SSRB sinogram with a span of 3 and ring difference of 31 and frame duration of 60 sec. was over 99.98% regardless of the acquisition time and over 97.50% for the SM. The accuracy of the sinogram method is slightly lower than the image method (approximately 2%), independently of total time acquisition. This can be explained by the fact that applying SDTT directly to the sinogram, there would be worse per-voxel statistics, and consequently low counts per voxel in the resultant images. IM is subsequently more accurate and practicable with regards to the time required to apply SDTT and the results achieved.

D. ^{18}F-FDG and ^{13}N-NH$_4^+$ concentrations

Table I presents ^{18}F-FDG and ^{13}N-NH$_4^+$ concentrations for IM, using a SSRB sinogram with a span of 3 and ring difference of 31, total time acquisition of 30 min and frame duration of 60 sec. As it can be observed, the resultant concentrations after applying SDTT are quite similar compared to the theoretical ones, the true concentration of each one is recovered. When one of the radiotracers is in majority, the recovered concentration value is better than when the radiotracers concentration is similar. When both radiotracers are in the same proportion, when SDTT is applied the ^{13}N-NH$_4^+$ signal will include most of image noise, because of its worse counts per voxel. When one of the radiotracers is in majority this *error* also exists but it has less impact at the resultant images.

The main factor influencing the performance of the SDTT is the per-voxel counting statistics. Nowadays, scanner sensitivities are higher comparing to those by the time which SDTT was originally proposed [4, 11, 12]. Higher sensitivity provides better per-voxel statistics and subsequently, current PET scanners enable the use of this technique. Nevertheless, sensitivity increase is partially counter-balanced because of spatial resolution improvement. Current PET scanners also present better spatial resolution, enabling smaller voxel sizes and therefore, rendering lesser counts per voxel at a certain activity concentration. Thus, even with higher sensitivity, the better per-voxel statistics achieved are also dependent of scanner spatial resolution, and therefore, voxel size [12-14]. In this study, for an acquisition of 20 and 30 min, approximately 9-13 and 13-19 x10^6 prompts were achieved.

Table I. Percentage of ^{18}F-FDG and ^{13}N-NH$_4^+$ concentrations of all the ROIs: the IM and theoretical results. The last column shows the percentage of the difference between the IM and the theoretical results.

	Image Method Results (IM)		Theoretical Results (Th.)		
ROI	%FDG	%NH$_4^+$	%FDG	%NH$_4^+$	%Diff.
1	91,79	8,21	90,67	9,33	-1,12
2	101,06	-1,06	100,00	0,00	-1,06
3	72,49	27,51	74,45	25,55	1,96
4	48,97	51,03	56,43	43,57	7,46
5	27,78	72,22	32,69	67,31	4,91
6	-0,1	100,1	0	100	0,09
background	50,07	49,93	50,00	50,00	-0,07

SDTT was applied using a rodent system. To apply SDTT using human scanners, the number of coincidence events on human imaging voxel must be the same as those achieved on a typical rodent imaging "voxel". Beyond the difference between human and rodent scanners regarding to spatial resolution and sensitivity, there is another limitation on human studies: the injected radiotracer concentration. Moreover, the injected radiotracer concentration used in this work is higher than those used on human studies. Consequently, the per-voxel coincidence events achieved in this work were higher than those usually used for human studies. To achieve a reasonable per-voxel counting statistics on human scanners and consequently a reasonable SDTT performance, an increase in sensitivity or an increase in voxel size, would be required.

IV. CONCLUSIONS

This study demonstrates that SDTT is practicable in rodent scanners and its precision depends on the experimental settings. Nowadays, the current PET scanners are more sensitive and provide better image resolution than when this technique was originally proposed in 1982 [4]. This procedure has not been routinely applied since that time because it may enhance noise in the images. However, in this study it was demonstrated that when a high per-voxel couting statistics is achieved SDTT is applicable. This can be achieved by applying SDTT using the SSRB with a span of 3 and a ring difference of 31, and acquire over 20 min, this technique discriminates both radiotracer images with similar SNR values comparing to the initial dynamic image. Subsequently, it can be concluded that SDTT does not enhance noise significantly

in the resultant images when the experimental settings are correctly chosen: total time acquisition and rebinning algorithm.

The SDTT procedure presented here has its own limitations. SDTT assumes that tracer concentrations do not change during the acquisition, therefore for kinetic studies SDTT is not applicable. SDTT can only be applied in static studies and the time acquisition of the experiment has to be at least 20 min. Lower time acquisition will generate noisier images. Nevertheless, these restrictions are identical as those usually met in diagnostic PET protocols using ^{18}F-FDG or ^{13}N-NH$_4^+$.

The use of SDTT in data acquired with human scanners would require of better per-voxel counting statistics, only attainable by increasing the sensibility of the tomograph, increasing its voxel size, and therefore worsening its spatial resolution, or increasing the acquisition time.

Future work will focus on applying and evaluating this technique using *in vivo* data, as well as, evaluating the role of iterative reconstruction algorithms, such as an ordered subsets-expectation maximization (OSEM) algorithm.

References

[1]   H. Kiat, G. Germano, J. Friedman, K. Van Train, G. Silagan, F. P. Wang, J. Maddahi, and D. Berman, "Comparative feasibility of separate or simultaneous rest thallium-201/stress technetium-99m-sestamibi dual-isotope myocardial perfusion SPECT," *J Nucl Med,* vol. 35, pp. 542-8, Apr 1994.

[2]   M. Unlu, S. Gunaydin, N. Ilgin, S. Inanir, N. Gokcora, and L. Gokgoz, "Dual isotope myocardial perfusion SPECT in the detection of coronary artery disease: comparison of separate and simultaneous acquisition protocols," *J Nucl Biol Med,* vol. 37, pp. 233-7, Dec 1993.

[3]   Y. W. Wu, P. J. Huang, C. M. Lee, Y. L. Ho, L. C. Lin, T. D. Wang, S. S. Wang, T. H. Chen, and R. F. Yen, "Assessment of myocardial viability using F-18 fluorodeoxyglucose/Tc-99m sestamibi dual-isotope simultaneous acquisition SPECT: comparison with Tl-201 stress-reinjection SPECT," *J Nucl Cardiol,* vol. 12, pp. 451-9, Jul-Aug 2005.

[4]   S. C. Huang, R. E. Carson, E. J. Hoffman, D. E. Kuhl, and M. E. Phelps, "An investigation of a double-tracer technique for positron computerized tomography," *J Nucl Med,* vol. 23, pp. 816-22, Sep 1982.

[5]   J. Verhaeghe, Y. D'Asseler, S. Staelens, and I. Lemahieu, "Noise Properties of Simultaneous Dual Tracer PET Imaging," *IEEE Nuclear Science Symposium,* vol. San Juan (Puerto Rico), 2005.

[6]   N. F. Black, S. McJames, T. C. Rust, and D. J. Kadrmas, "Evaluation of rapid dual-tracer (62)Cu-PTSM + (62)Cu-ATSM PET in dogs with spontaneously occurring tumors," *Phys Med Biol,* vol. 53, pp. 217-32, Jan 7 2008.

[7]   Y. Ikoma, H. Toyama, and T. Suhara, "Simultaneous quantification of two brain functions with dual tracer injection in PET dynamic study," in *Quantitation in Biomedical Imaging with PET and MRI*, 2004, pp. 74-78.

[8]   T. C. Rust and D. J. Kadrmas, "Rapid dual-tracer PTSM+ATSM PET imaging of tumour blood flow and hypoxia: a simulation study," *Phys Med Biol,* vol. 51, pp. 61-75, Jan 7 2006.

[9]   J. W. Wilson, T. G. Turkington, J. G. Colsher, S. Borges-Neto, R. E. Reinman, and E. Coleman, "Optimizing Sequential Dual Tracer PET Studies using combined 2D/3D Imaging Protocol," in *IEEE Nuclear Science Symposium*, Rome (Italy), 2004.

[10]   J. M. Baron, I. G. Zubal, L. Daley, C. Ng, H. Dey, and J. Seibyl, "Simultaneous High Resolution Dual Isotope F18 PET and Tc99m SPECT with Cross-talk Correction," *Clin Positron Imaging,* vol. 1, p. 251, Sep 1998.

[11]   P. E. Valk, L. Dale, D. Bailey, D. W. Townsend, and M. N. Maisey, *Positron Emission Tomography: Basic Science and Clinical Practice* London: Springer, 2004.

[12]   J. J. Vaquero and M. Desco, "[Technical limitations of the positron emission tomography (PET) for small laboratory animals]," *Rev Esp Med Nucl,* vol. 24, pp. 334-47, Sep-Oct 2005.

[13]   E. M. Jagoda, J. J. Vaquero, J. Seidel, M. V. Green, and W. C. Eckelman, "Experiment assessment of mass effects in the rat: implications for small animal PET imaging," *Nucl Med Biol,* vol. 31, pp. 771-9, Aug 2004.

[14]   S. C. Strother, M. E. Casey, and E. J. Hoffman, "Measuring PET scanner sensitivity: relating count rates to image signal-to-noise ratios using Noise Equivalent Counts," in *IEEE T Nucl Sci.* vol. 37:783-8, 1990.